EIGHTH EUROPEAN ROTORCRAFT FORUM

Paper No 2.2

DEVELOPMENT OF NEW AIRFOIL SECTIONS FOR HELICOPTER ROTOR BLADES

K.H. HORSTMANN, H. KÖSTER

DFVLR, Germany

G. POLZ

MBB, Germany

August 31 through September 3, 1982

AIX-EN-PROVENCE, FRANCE

ASSOCIATION AERONAUTIQUE ET ASTRONAUTIQUE DE FRANCE

DEVELOPMENT OF NEW AIRFOIL SECTIONS FOR HELICOPTER ROTOR BLADES

K.H. Horstmann, H. Köster
Deutsche Forschungs- und Versuchsanstalt für Luft- und Raumfahrt e.V. (DFVLR)
Braunschweig, Germany

G. Polz
Messerschmitt-Bölkow-Blohm GmbH
München, Germany

Abstract

In cooperation between DFVLR and MBB two new advanced airfoils for helicopter rotor blades have been developed and investigated in the wind tunnel.

Starting from the requirements of the helicopter rotor depending on the missions to be performed the design objectives for the blade sections in several rotor stations are described. The used iterative design procedure consisting of a subsonic design code and a transonic analysis code is shortly explained and some essential features of the shape of such airfoils are commented. The main results of the experimental investigations of the new developed airfoils having thickness to chord ratios of t/c = 0.09 and 0.12 are discussed and compared with those of other airfoils and with calculations.

1. Introduction

An airfoil with good aerodynamic characteristics forms the basis of a successful rotor design. The development of more efficient airfoils for helicopter rotor blades is therefore an essential task for improving helicopter rotor performance and for extending the flight envelope of helicopters.

Whereas the first built helicopter rotors were equipped with symmetrical airfoils, which have the advantage of a zero pitching moment at zero lift like the well known NACA 0012, cambered airfoils have been introduced for the second helicopter generation. This was the most significant progress for rotor airfoils. NACA 23012 wing section and its derivatives are for example often used airfoils of this kind. The use of camber improved rotor performance in hover and forward flight involved, however, increased blade and control loads.

The second significant step was the introduction of transonic airfoils with improved behaviour due to local supersonic flow. The development of the first transonic airfoils have been carried out only by experimental investigations. The growing understanding of transonic flow and the progress in the field of numerical methods in the last decade especially for the computation of transonic flow and in the coupling of inviscid flow calculation and viscous correction now allows the design of airfoils to an accuracy high enough to supply essential improvements of aerodynamic behaviour as far as attached flow is concerned.

Appointing well-founded design objectives is another important condition for a sucessful airfoil design. This requires a good knowledge of the rotor flow environment, a detailed analysis of the missions to be performed by the helicopter under consideration, taking into account the limitations of the applied design methods for two-dimensional flow, and the accuracy of the test facility. In ref. [1] to [11] the problems of rotor airfoils are discussed in detail.

In 1981 a cooperation has begun between the Institut for Design Aerodynamics of the DFVLR and the Helicopter Divison of MBB for developing advanced airfoils for new helicopter rotors. The design objectives have been stated by MBB in consideration of the missions to be performed and of their rotor flow

calculations. Design of rotor airfoils, manufacturing of wind tunnel models, and experimental investigations habe been accomplished by DFVLR.

2. Design objectives for helicopter rotor airfoils

In addition to the global requirements on rotor airfoils, as low drag at high Mach numbers and high lift capability at lower Mach numbers, detailed design objectives for the development of new airfoils can be found in a number of papers [1] to [11] handling the design of rotor airfoils. Usually these objectives are obtained for specific rotor configurations.

Because a new developed airfoil (or airfoil family) during it's life span will be applied on different rotor configurations, an overview of the whole field of operational conditions for rotor airfoils seems to be important before starting with the airfoil design. Decisive flight conditions influencing the airfoil design are:

- hover flight
- forward flight at maximum cruise speed
- forward flight at the speed for maximum range
- maneuver flight with load factors > 1

The operational conditions of rotor airfoils can be specified by the following parameters:

- rotor tip speed
- radial position of the desired blade section
- blade twist
- rotor disc area loading
- rotor solidity
- inclination of the blade tip plane
- flight speed
- atmospheric conditions

From these parameters the inclination of the blade tip plane against the flight path is primarily a characteristic of the specific helicopter design, because it depends overwhelmingly on the total drag area of the helicopter.

Fig. 1 shows the variety of values of the tip plane inclination angle γ vers. flight speed V for typical helicopters at maximum gross weight. The γ values range from 4° up to 9°. It should be considered that for each helicopter the inclination angle increases for lower gross weights. Additionally marked in fig.1 are the regions for optimum cruising speed (at optimum range) and for maneuver flight with maximum possible load factor.

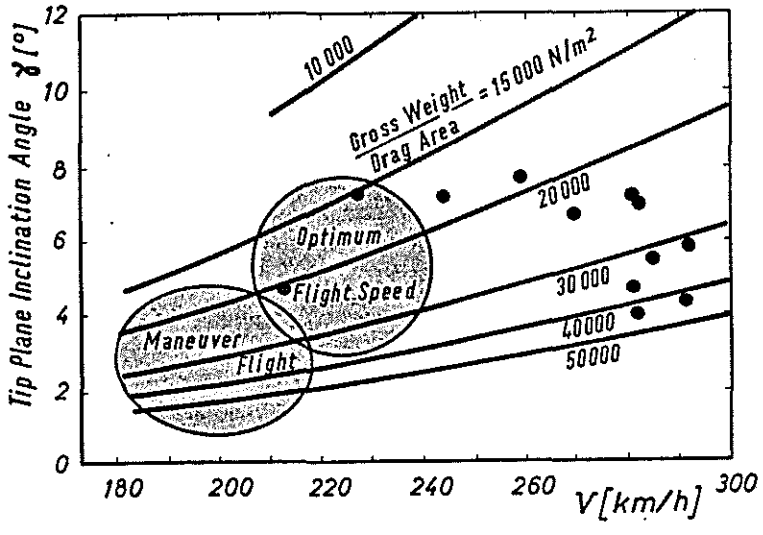

Fig. 1 Tip plane inclination angles of different helicopter types at maximum horizontal speed

The effects of the tip plane inclination can be seen in fig.2 where the ratio of local lift coefficient c_L and mean lift coefficient $\bar{c}_L$ is shown as a function of the advance ratio μ for azimuthal positions of 0°, 90° and 270° respectively. Radial blade positions of 95 and 80% blade radius are considered here

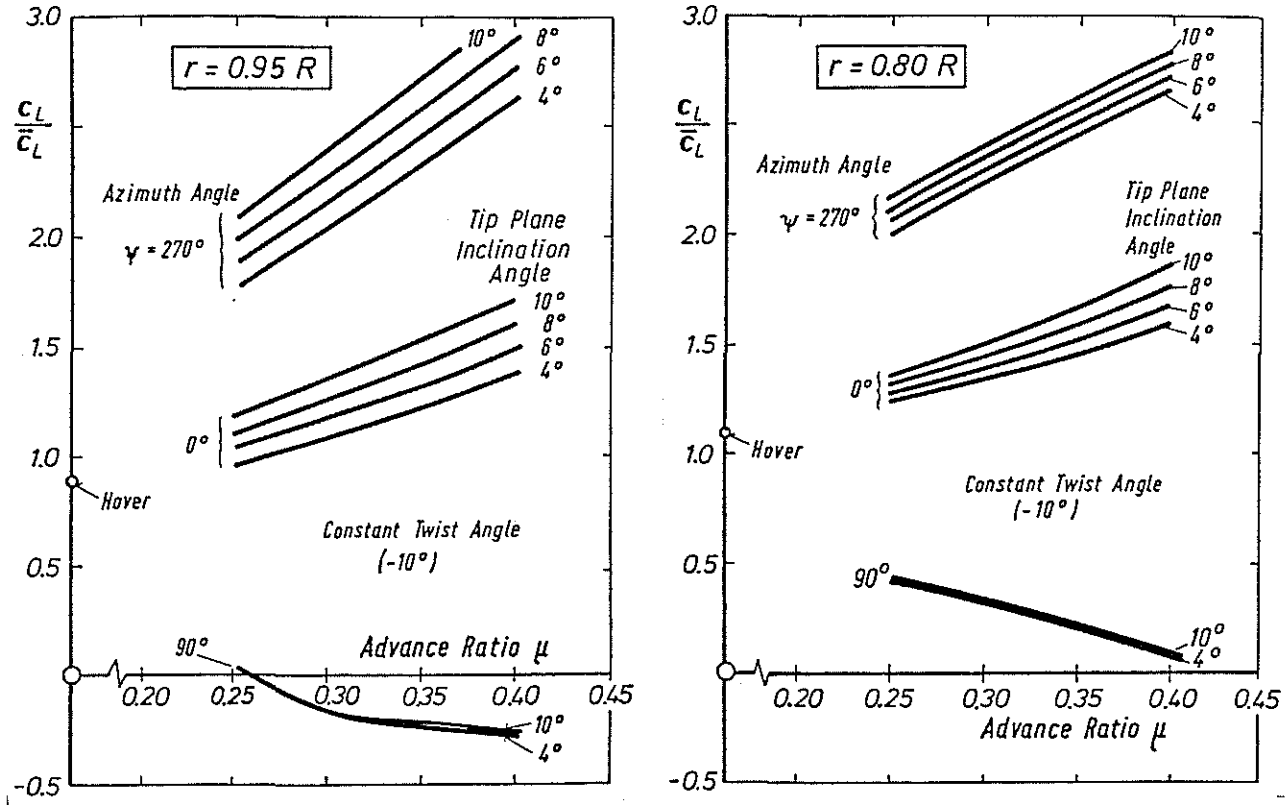

Fig. 2 Tip plane inclination effects on blade lift coefficient for radial positions of 0.95 and 0.8 R

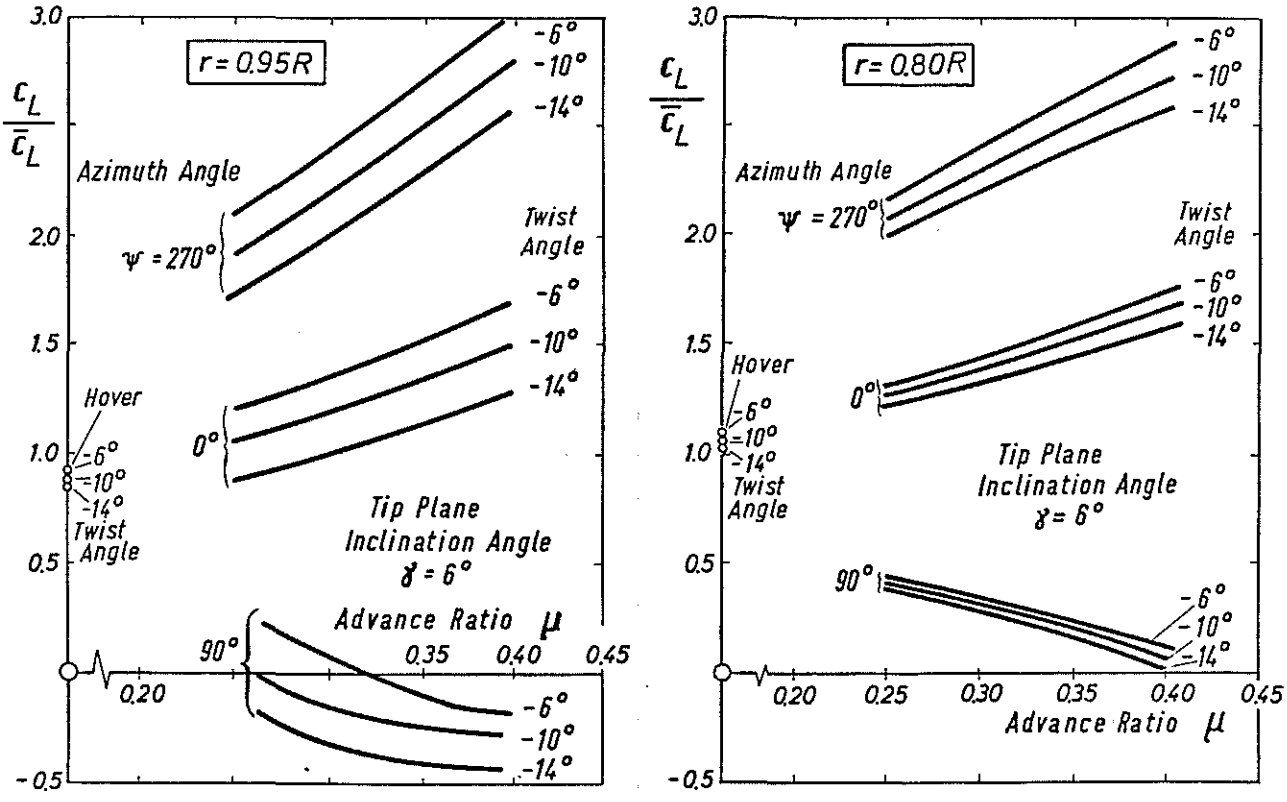

Fig. 3 Blade twist effect on blade lift coefficient for radial positions of 0.95 and 0.8 R

to achieve the design objectives for a tip airfoil as well as for an airfoil for the inner blade regions. The curves in fig. 2 are the result of a number of rotor calculations whereby the tip speed and the rotor solidity are varied over a broad range to cover the operational conditions of different rotor configurations. An artificial non-stalling airfoil polar is applied for these calculations. Due to the reduction of the lift data with the mean lift coefficient the influence of the tip plane inclination in fig. 2 is independent from the tip speed and the rotor solidity.

In a similar manner the influence of the blade twist angle is determined for constant tip plane angle (fig. 3). Within the range of usual rotor design the effects of the blade twist seem to be more dominant than those of the tip plane inclination.

On the basis of the results in fig. 2 and 3 the main operational conditions (lift coefficient c_L, Mach number M) of the airfoil sections at 80% and 95% blade radius can be determined for a specific helicopter configuration (flight speed, tip plane inclination) and rotor design (tip speed, blade twist, solidity). To achieve quantitative design objectives for the airfoil development, the airfoil operational conditions are specified in a helicopter design study for the prevailing flight conditions described above. From those data the operational conditions can be determined for the whole Mach number range (fig. 4 and 5).

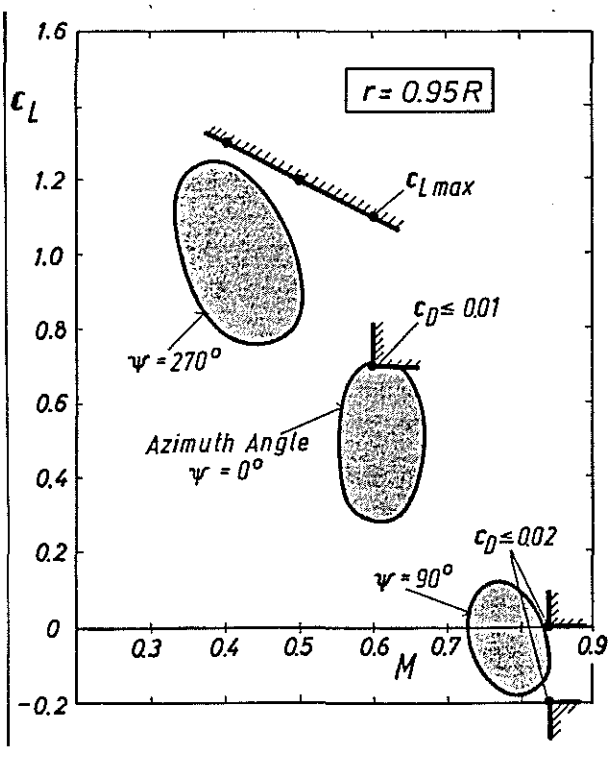

Fig. 4 Design objectives for the tip airfoil

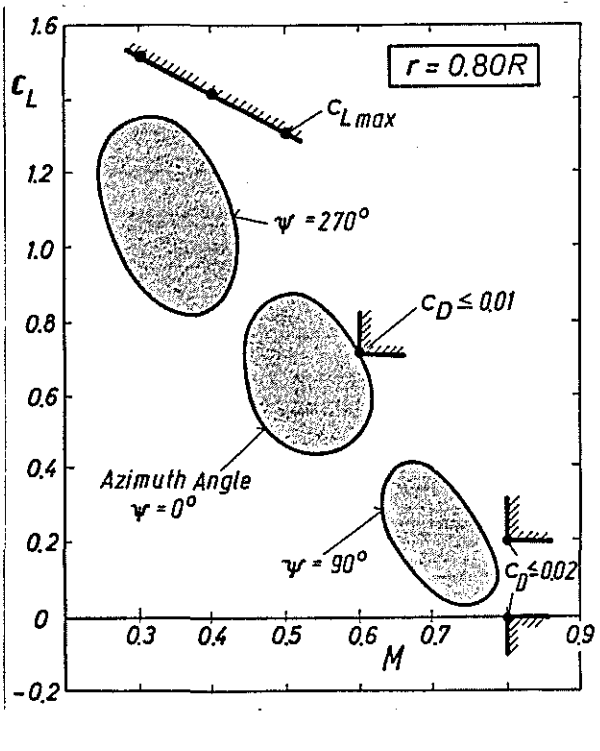

Fig. 5 Design objectives for the airfoil for the inner blade parts

The design objectives for both airfoils can be stipulated as follows:

design objective	inner airfoil	tip airfoil
thickness	12%	9%
drag divergence ($c_D = 0.02$)	$M > 0.8$ at $c_L = 0/0.2$	$M > 0.84$ at $c_L = -0.2/0$
drag at $M = 0.6$, $c_L = 0.7$	$c_D \leq 0.01$	$c_D \leq 0.01$
maximum lift at $M = 0.3$ $M = 0.4$ $M = 0.5$	$c_{Lmax} = 1.5$ 1.4 1.3	$c_{Lmax} = 1.3$ 1.2
pitching moment below stall inception	$\lvert c_m \rvert \leq 0.01$	$\lvert c_m \rvert \leq 0.01$

3. Airfoil design

Realizing the above design objectives two methods are used. The inverse problem which needs the prescribed velocity distribution on the airfoil as input and which leads to the airfoil contour and to the aerodynamic coefficients has been solved by a modified computer code from Eppler and Somers [12]. This very efficient code for incompressible flow has been extended to subsonic flow by Radespiel [13] who introduced a combination of two different compressibility rules. The Eppler/Somers code bases on a conformal mapping procedure in its design part and on a higher order panel/boundary layer interaction method in its analysis part. A number of options can be specified in the design part such as extent of upper and lower surface pressure plateau at specified angle of attack, extent and behaviour of recompression in the rear part, trailing edge angle, etc..

For transonic flow the Bauer/Garabedian/Korn/Jameson method (BGK III) was used [14], [15] which bases on a finite difference approximation of the full potential equation in a transformed mesh to fulfill the exact boundary conditions. In the BGK III as well as in the modified Eppler/Somers code the viscous effects are taken into account by adding the boundary layer displacement thickness to the airfoil contour.

Both codes cannot predict the maximum lift coefficient c_{Lmax} because they are unable to calculate separated flow regions. For the estimation of c_{Lmax} values the following auxiliary criterions are used. At Mach number of $M = 0.3$ c_{Lmax} is reached when the pressure coefficient at the calculated separation point is equal zero. At $M = 0.4$ either the above separation criterion or a limiting maximum local Mach number of 1.4 was used. Maximum lift coefficient at $M = 0.5$ was estimated by limiting the local Mach number just ahead of the shock pressure rise to a value of 1.4.

With these methods the different steps in the design process are:

1. Choice of a prescribed velocity distribution or change of a velocity distribution used in a step before.
2. Calculation of airfoil contour and aerodynamic coefficients at main design objectives by means of the subsonic code (computer time: a few seconds).
3. Reiteration of step 1 and 2 until the desired subsonic airfoil characteristics are obtained.

4. Calculation of the transonic behaviour at all design objectives by means of the Bauer/Garabedian/Korn III method (computer time: ~ 80 s for one pressure distribution).

5. Reiteration of step 1 to 4 until the desired subsonic and transonic behaviour is obtained.

This iterative design procedure seems to be more efficient than the use of a current transonic design method especially in the case of a rotor airfoil in which a lot of adverse requirements must be taken into account.

Realizing these requirements it is convenient to use design features based on physical understanding of the flow concerning the pressure distribution resp. the contour curvature. These design features are published by several authors as Wortmann [2], [3], Dadone [6], Thibert [7]. Some of the features may shortly be summarized here:

- minimize the shock wave strength by
  - small contour curvature in the regions of supersonic flow in the cases of low lift and high Mach number as well as in the case of high lift and M = 0.4 and 0.5
  - avoiding of high contour curvature in front of and at the beginning of supersonic flow regions in order to get a low level of local Mach number
- high maximum lift coefficient at M = 0.3 by reducing the maximum velocity near the leading edge
- low drag at M = 0.6 and $c_L \approx 0.6$ by extending the laminar flow regions especially on lower side (other requirements do not allow this on upper side)
- lower side front loading and reflexed meanline near trailing edge to reduce moment coefficients c_m
- using a tab to move the aerodynamic center (a.c.) backwards and to reduce the band-width of c_m values.

All the above mentioned characteristics are mainly influenced by limited contour regions. These regions lie very close together resp. they are overlapping each other especially on the upper surface between leading edge and 40% chord length where rotor airfoil design seems to be a balance act in distributing the contour curvature in view of the design objectives at a given thickness ratio.

4. Results

4.1 Windtunnel

The experimental investigations have been carried out in the Transonic Windtunnel Braunschweig (TWB) of the DFVLR [16]. The windtunnel is of the blow-down type and especially suited for airfoil tests at subsonic and transonic flows in the Mach number range of M = 0.3 to 0.9. The rectangular test section of 34 cm by 60 cm (fig. 6) with slotted walls at the top and the bottom allows testing of airfoil models with chord lengths of 10 cm to 20 cm and a span of 34 cm. This results in

- windtunnel height/ airfoil chord ratios of 6.0 to 3.0
- and geometric aspect ratios of 3.4 to 1.7

which are usual for airfoil investigations. In this case 15 cm chord length models have been used. The width of the slots has been optimised for zero blockage corrections. This has led to an open area ratio of 2.35%. With a maximum pressure in the test section of 4.5 bars and a chord length of 15 cm a Reynolds number of $Re = 10^7$ can be achieved.

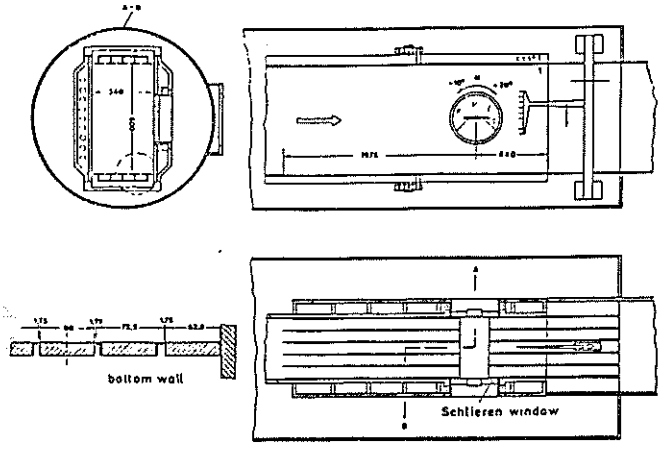

Fig. 6 Transonic Windtunnel Braunschweig (TWB) of DFVLR

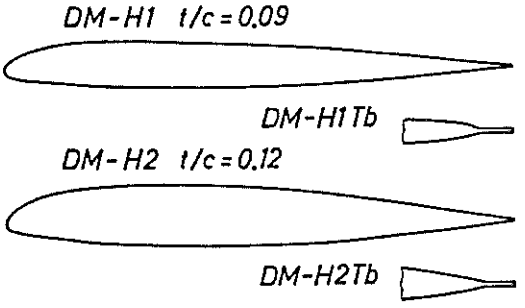

Fig. 7 Helicopter rotor blade airfoils DM-H1 and DM-H2

In a routine investigation the subsequent data are provided from the experiment

- static pressure on the airfoil contour in approximately 50 points on the contour
- total and static pressure in the wake at approximately 360 points.

Lift and pitching moment coefficient are evaluated from the contour pressure, drag coefficient from the wake traverse pressures.

4.2 Experimental Results

The contours of the two airfoils DM-H1 and DM-H2 designed by the previous described methods are shown in fig. 7. Their thickness to chord ratios are t/c = 0.09 and 0.12. Also shown are the tab versions designated by DM-H1 Tb and DM-H2 Tb. The shape of the tabs follows essentially the experimental investigations of [17]. The tab lengths amount to 5% of chord length for the DM-H1 Tb and to 4% for the DM-H2 Tb airfoil. All windtunnel tests have been carried out without transition strip on these airfoils.

The total performances of the two airfoils in the tab version resulting from the experimental investigations in the TWB are summarized in the figs. 8 and 9 in lift coefficient vers. Mach number diagrams presenting the maximum lift coefficient, the drag divergence Mach number M_{DD} defined by $dC_D/dM = 0.1$ at constant lift level, and lines of constant drag coefficient of $c_D = 0.01$ and 0.02. For the DM-H1 Tb airfoil a maximum lift coefficient at M = 0.4 of $c_{Lmax} = 1.31$ and a drag divergence Mach number at zero lift of $M_{DDo} = 0.82$ is achieved. The corresponding values for the DM-H2 Tb airfoil are $c_{Lmax} = 1.52$ at M = 0.3, 1.36 at M = 0.4 and 1.28 at M = 0.5 and $M_{DDo} = 0.805$.

The pitching moment coefficients at zero lift c_{mo} in dependance of Mach number for the two airfoils with and without tabs are compared on fig. 10. The c_{mo} values for the tab versions are sligthly shifted in the positive direction. The effect of the tabs on the pitching moment c_m with increasing lift coefficient at constant M = 0.4 is shown in fig. 11. The slope of the c_L, c_m curve is changed and the requirement of $|c_m| \leq 0.01$ is fulfilled in nearly the whole c_L range.

As an example the measured drag polars for the Mach number M = 0.6 at a Reynolds number $Re = 4.8 \cdot 10^6$ are given in fig. 12. For the H1 Tb airfoil a minimum drag coefficient of $c_D \approx 0.007$ respectively $c_D = 0.0078$ for the airfoil

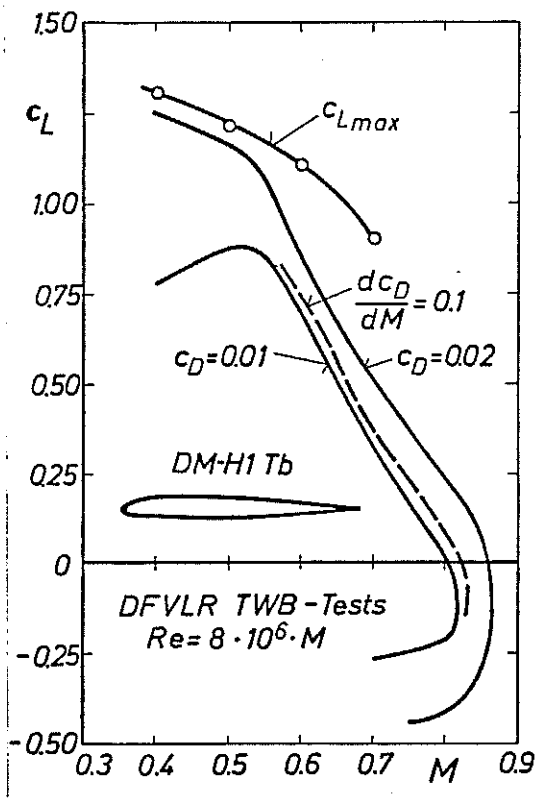

Fig. 8 Measured performance boundaries of the airfoil DM-H1 Tb

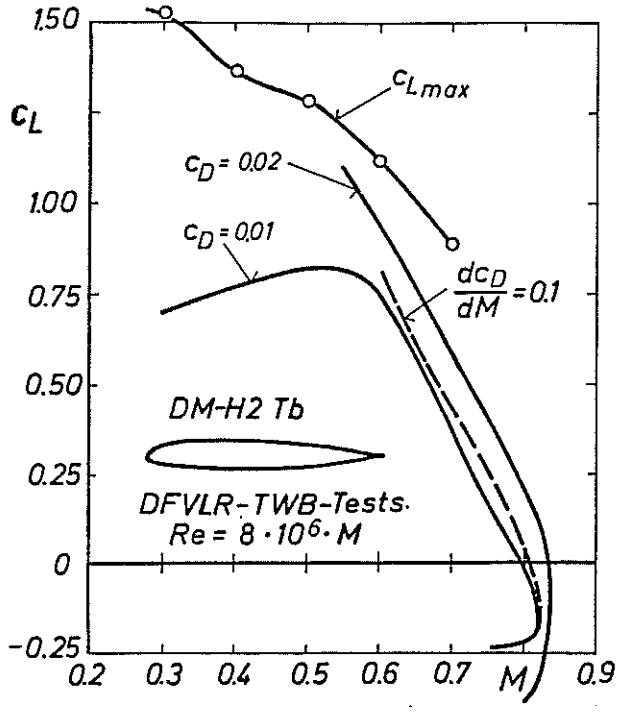

Fig. 9 Measured performance boundaries of the airfoil DM-H2 Tb

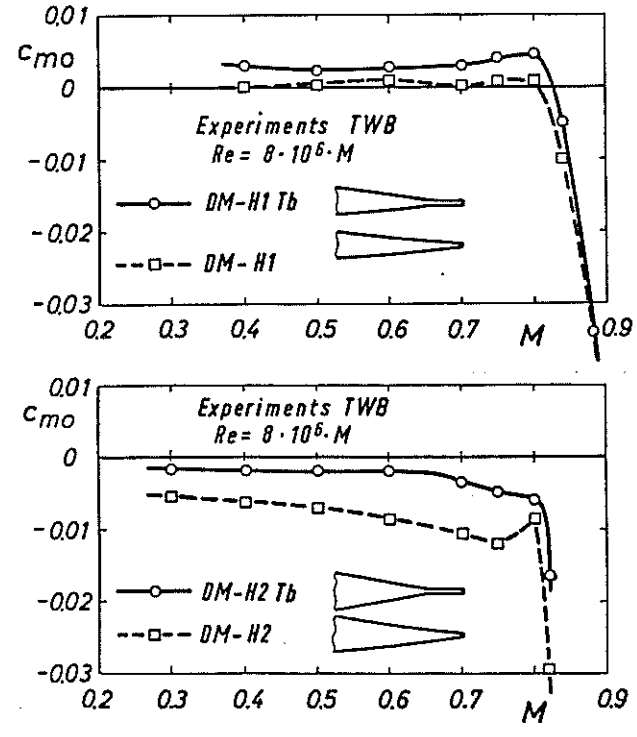

Fig. 10 Tab influence on zero lift pitching moment coefficient

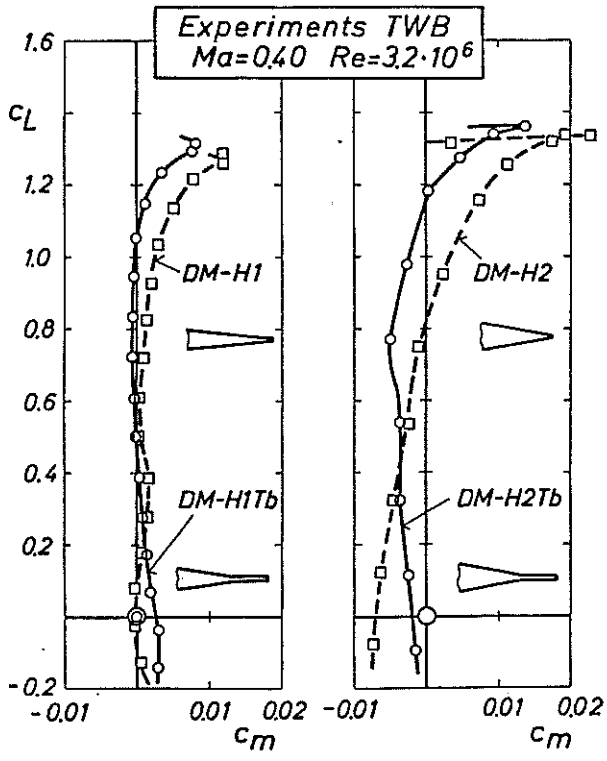

Fig. 11 Tab influence on pitching moment evolution

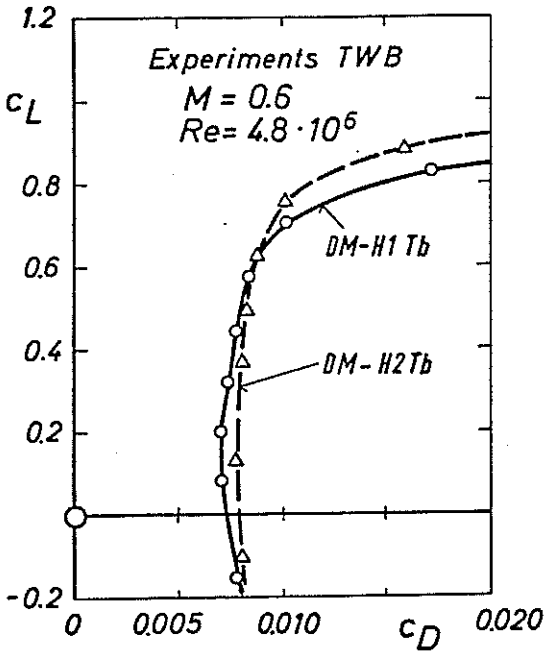

Fig. 12 Drag polars of the airfoils DM-H1 Tb and DM-H2 Tb

	Airfoil	Tunnel	Re·10⁻⁶	Transition
—△—	DM-H2 Tb	TWB	4.8	natural
-----	OA 212	S3 MA	4.2	natural
-------	23012 5% Tab	ARA	4.2	fixed

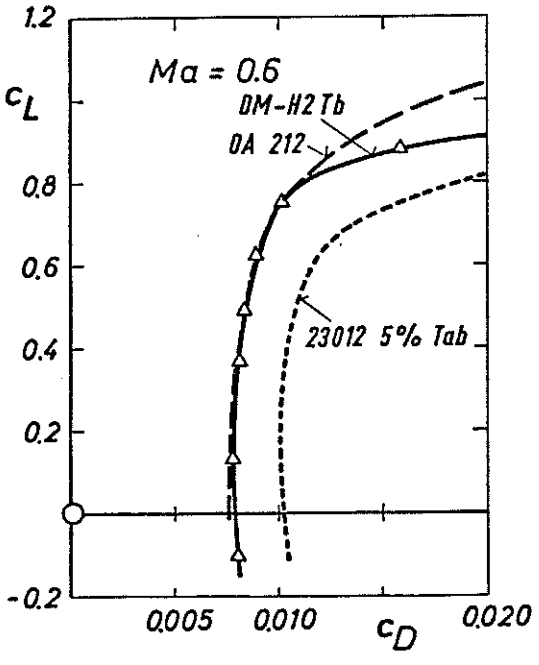

Fig. 13 Drag polars of several airfoils at M = 0.6

H2 Tb are measured. Due to greater thickness the airfoil H2 Tb has a higher drag level but compared to airfoil H1 Tb the low drag values extend to higher lift coefficients. For c_L = 0.7 lift/drag ratios of c_L/c_D = 70 respectively 74 are achieved.

Comparing these results with the design objectives discussed in chapter 2 it can be seen that the new developed airfoils are fulfilling almost completely the stated requirements in regard of aerodynamic performances and moment behaviour. Only the $c_{L_{max}}$ value of the H2 Tb airfoil at M = 0.4 should be somewhat higher. It seems, however, to be possible to improve it because the good high speed performances for negative lift coefficients can be reduced for a small amount.

4.3 Comparison with other airfoils

It has to be mentioned that it is always problematic to compare results of airfoil tests being made in different windtunnels and in addition for various Reynolds numbers especially concerning drag and maximum lift coefficient. For comparison test results of the airfoils OA 209 and OA 212 from the S3 MA windtunnel in Modane [7],[8], [9] and results of the airfoil NACA 23012 fitted with a 5% tab and transition strips between 8% and 9% of the chord on lower and upper side from the ARA windtunnel [18] have been chosen.

In fig. 13 the drag polars of the three airfoils DM-H2 Tb, OA 212 and NACA 23012 (5% Tab) at a Mach number M = 0.6 are presented. Up to a lift coefficient of c_L = 0.8 both the DM-H2 Tb and OA 212 airfoils have nearly the same values. For $c_L > 0.8$ the drag of the DM-H2 Tb airfoil increases more rapidly than that of the OA 212 airfoil. One possible reason for this behaviour is the presence of a separation bubble which is growing with increasing lift. Assuming that the drag at low lift coefficient with regard to the transition strip

is equal to the two others the NACA 23012 (5% Tab) is producing more drag for $c_L > 0.5$. The comparison of the zero lift drag coefficient c_{Do} of these airfoils plotted against Mach number on fig. 14 shows that a higher drag divergence Mach number for the DM-H2 Tb of more than $\Delta M_{DD} = 0.02$ has been obtained. The same comparison on fig. 15 between the DM-H1 Tb and OA 209 airfoils indicates that the drag divergence Mach number for the DM-H1 Tb is less than that of the OA 209 which on the contrary shows some drag creep.

	Airfoil	Tunnel	$Re \cdot 10^{-6}$	Transition
—△—	DM-H2 Tb	TWB	8·M	natural
——	OA 212	S3MA	7·M	natural
-------	23012 5% Tab	ARA	7·M	fixed

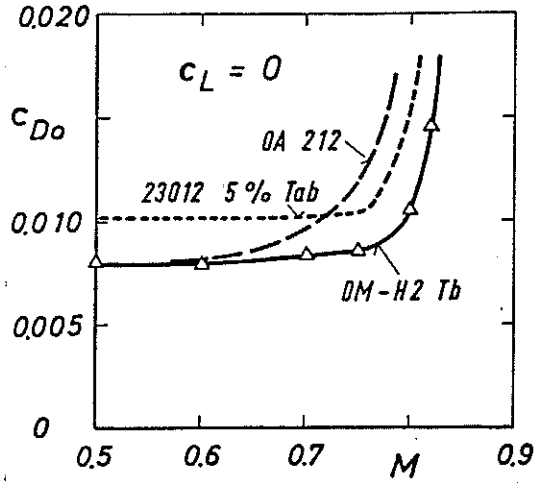

Fig. 14 Zero lift drag coefficients of several airfoils

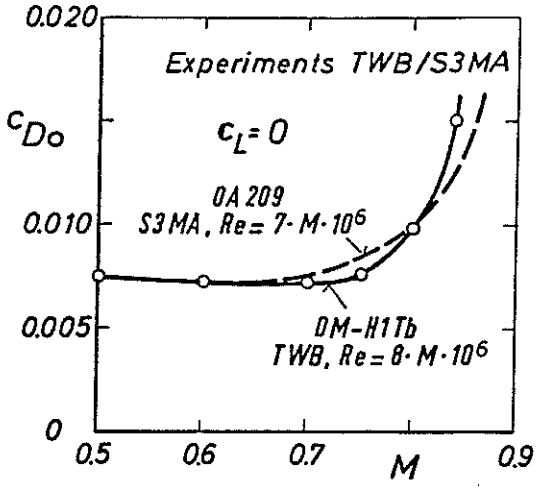

Fig. 15 Zero lift drag coefficients of the airfoils OA 209 and DM-H1 Tb

The c_m evolution with lift coefficient at M = 0.5 on fig. 16 for the DM-H1 Tb and OA 209 airfoils shows nearly a similar behaviour. The c_m values do not exceed ±0.01 up to values of $c_L \sim 1.1$. Only the DM-H1 Tb reaches $c_m \simeq 0.02$ but for the higher value of $c_{Lmax} = 1.22$. Fig. 16 presents also the c_m evolution with c_L at M = 0.3 for the DM-H2 Tb and OA 212 airfoils. The range of c_m for DM-H2 Tb airfoil extends from -0.006 to 0.011 and for the OA 212 from -0.001 to -0.014 so that the latter reaches a slightly larger absolute value.

A comparison of the new airfoils with the OA-series and the NACA 23012 (5% Tab) in maximum lift coefficient vers. drag divergence Mach number diagrams is presented in fig. 17 for the Mach numbers M = 0.3, 0.4 and 0.5. The largest gain in c_{Lmax} and M_{DDo} is obtained for the DM-H2 Tb airfoil at M = 0.3, and though in all other cases better performances have been achieved it is desirable to shift the drag divergence Mach number of the DM-H1 Tb airfoil to a somewhat higher value.

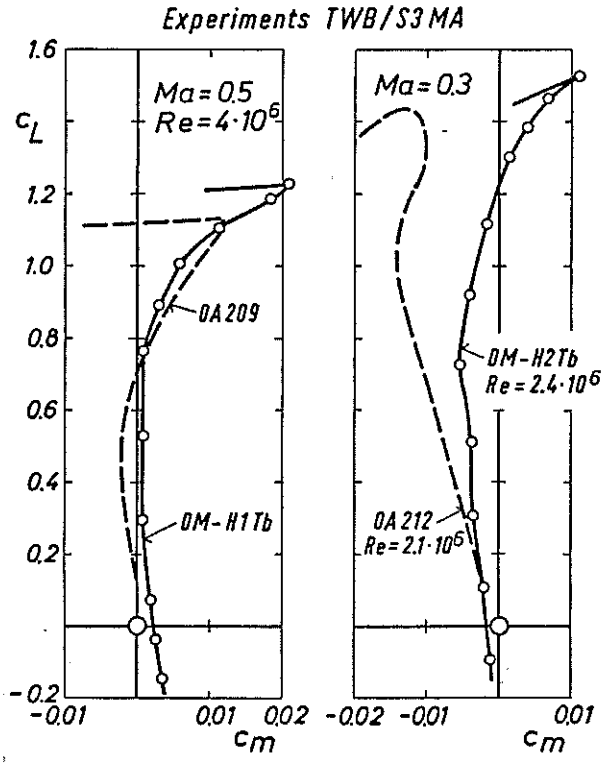

Fig. 16 Comparison of pitching moment coefficient evolution of several airfoils

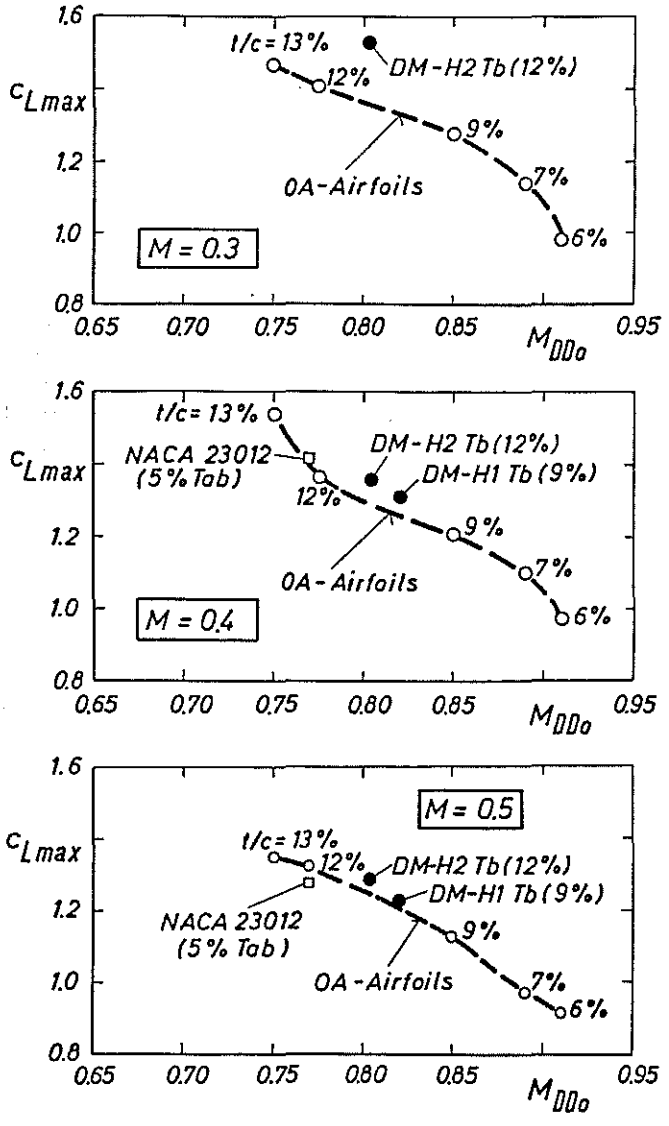

Fig. 17 Measured maximum lift coefficients and drag divergence Mach number of several rotor blade airfoils

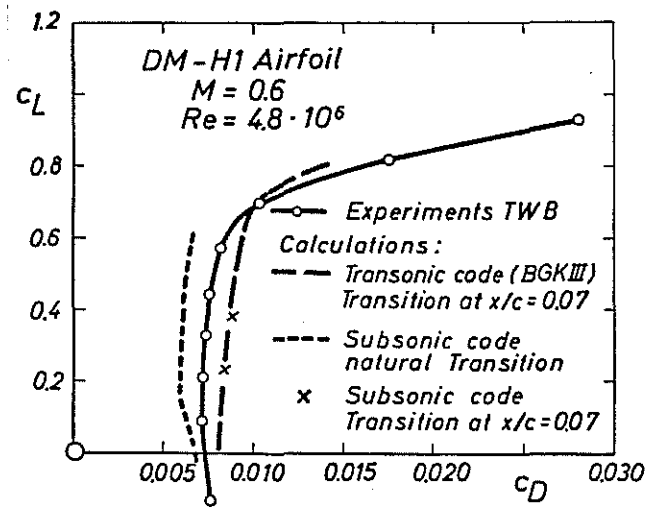

Fig. 18 Comparison of measured and calculated drag polars of the airfoil DM-H1 at M = 0.6

4.4 Comparisons between theory and experiment

Fig. 18 shows experimental and calculated polar curves of the DM-H1 airfoil at M = 0.6. It is remarkable that the measured drag values at lift coefficients up to 0.6 are higher than the calculated ones with natural transition but lower than the calculated values with transition at 7% chord length. This indicates that in the experiments at natural transition the extent of the laminar boundary is smaller than predicted by theory. This can have various reasons e.g. influence of windtunnel turbulence and noise level on transition or uncertainties in the calculation methods.

Comparison of theoretical and experimental polar curves in fig. 19 of the DM-H1 at M = 0.7 show a more rapid increasing drag coefficient of the experimental values at lift coefficients higher 0.3, whereas below this value due to different transition conditions the experimental values are lower than the calculated ones. The oil flow pattern in fig. 20 correlated to c_L = 0.5 in fig. 19 shows a shock induced separation bubble which might cause additional drag and which of course is not taken into account in the calculations.

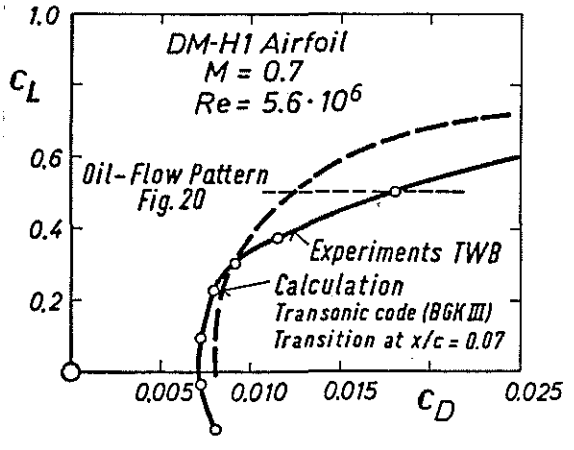

Fig. 19 Comparison of measured and calculated drag polars of the airfoil DM-H1 at M = 0.7

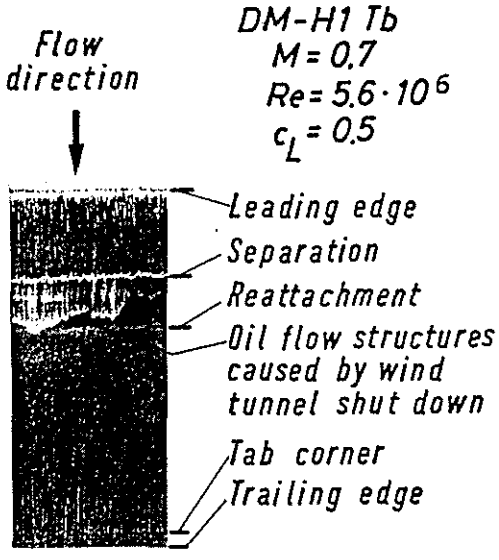

Fig. 20 Section of an oil flow pattern on the airfoil DM-H1 Tb

In fig. 21 and 22 which show zero lift drag coefficient and pitching moment coefficient vers. Mach number the calculated curves are in acceptable agreement with the experimental values especially when they are rapidly increasing due to increasing Mach number.

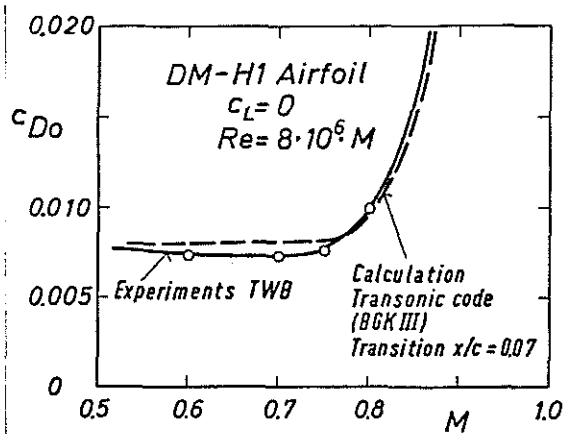

Fig. 21 Comparison of measured and calculated zero lift drag coefficients of the airfoil DM-H1

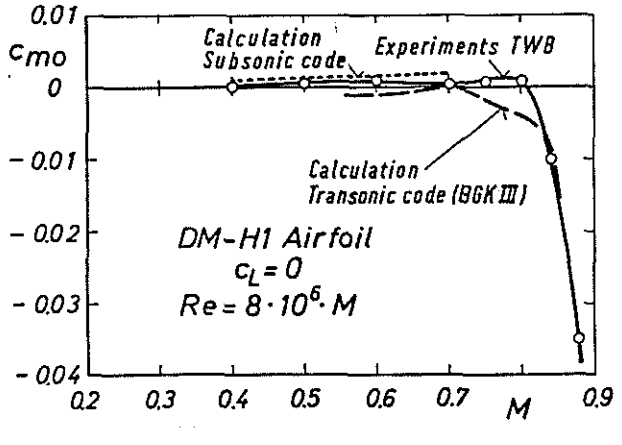

Fig. 22 Comparison of measured and calculated zero lift pitching moment coefficients of the airfoil DM-H1

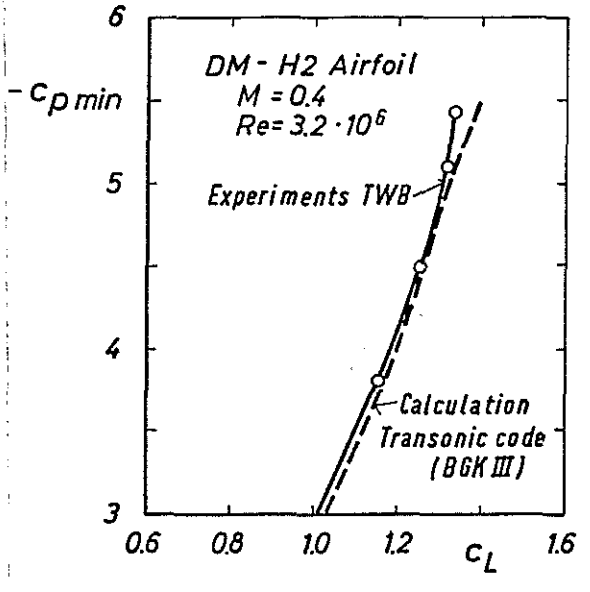

Fig. 23 Comparison of measured and calculated minimum pressure coefficient of the airfoil DM-H2

In fig. 23 showing minimum pressure coefficient c_{pmin} of the DM-H2 airfoil near leading edge vers. lift coefficient at M = 0.5 the agreement between measured and calculated values is rather good. The somewhat larger differences near c_{Lmax} are caused by trailing edge separation which is not taken into account in the used computer codes.

5. Conclusions

1. Design objectives for helicopter rotor airfoils are stated by means of detailed analysis of their operational conditions.
   Two airfoils have been designed. Aerodynamic behaviour and performances have been theoretically predicted and verified by 2d-windtunnel tests.

2. The combination of an efficient subsonic design method and a current transonic analysis code has been proved useful for rotor airfoil development.

3. By this first approach of rotor airfoil development in the DFVLR the state-of-the-art performance level has been obtained and the stated design objectives have essentially been fulfilled.

4. Theoretically predicted and measured values of aerodynamic coefficients show good agreement if no separated flow regions exist.

5. It seems to be possible to improve some characteristics of the two developed airfoils in view of a higher degree of adaption to rotor airfoil requirements.

References

[1] G. Reichert and S.N. Wagner, Some Aspects of the Design of Rotor Airfoil Shapes, AGARD-CP-111, 1973, Paper 14.

[2] F.X. Wortmann, J.M. Drees, Design of Airfoilsfor Rotors,Paper presented at the CAL/AVLABS 1969 Symposium on Aerodynamics of Rotary Wing and VTOL Aircraft, Buffalo, N.Y..

[3] J.W. Sloof, F.X. Wortmann, J.M. Duhon, The Development of Transonic Airfoils for Helicopters, Paper presented at the 31st Annual National Forum of the American Helicopter Society, Washington D.C., May 1975.

[4] R.W. Prouty, A State-of-the-Art Survey of Two-Dimensional Airfoil Data. AHS Symposium on Helicopter Aerodynamic Efficiency, March 1975.

[5] J. Renaud and F. Nibelle, Effects of the Airfoil Choice on Rotor Aerodynamic Behaviour in Forward Flight. Paper presented at the 2nd European Rotorcraft and Powered Lift Aircraft Forum, Bückeburg, September 1976.

[6] L. Dadone, Rotor Airfoil Optimization: An Understanding of the Physical Limits, Paper presented at the 34th Annual National Forum of the American Helicopter Society, May 1978, Washington D.C., Preprint 78-4.

[7] J.J. Thibert and J. Gallot, A New Airfoil Family for Rotor Blades, Paper presented at the 3rd European Rotorcraft and Powered Lift Aircraft Forum, Paper No. 41, Aix-en-Provence, September 1977, T.P. ONERA 1977-131

[8] J.J. Thibert and J. Gallot, Advanced Research on Helicopter Blade Airfoils, Paper presented at the 6th European Rotorcraft and Powered Lift Aircraft Forum, Paper No. 49, Bristol, September 1980, T.P. ONERA 1980-93.

[9] J.J. Thibert and J.M. Pouradier, Design and Test of a Helicopter Rotor Blade with Evolutive Profile, 12th ICAS Congress, Munich, October 1980, T.P. ONERA 1980-125.

[10] L. Dadone, The Role of Analysis in the Aerodynamic Design of Advanced Rotors, AGARD-CPP-334, Paper 1, May 1982.

[11] J.J. Thibert and J.J. Philippe, Etudes de Profiles et d'Extrêmités de Pale d'Hélicoptère, AGARD-CPP-334, Paper 3, May 1982.

[12] R. Eppler and D.M. Somers: A Computer Program for the Design and Analysis of Low-Speed Airfoils, NASA TM 80210, 1980.

[13] R. Radespiel: Erweiterung eines Profilberechnungsverfahrens im Hinblick auf Entwurfs- und Nachrechnungen von Laminarprofilen bei Verkehrsflugzeugen, DFVLR IB 129-81/15, 1981.

[14] F. Bauer, P. Garabedian, D. Korn, A. Jameson, Supercritical Wing Sections II, Springer-Verlag, Berlin, Heidelberg, New York, 1975.

[15] F. Bauer, P. Garabedian, D. Korn, Supercritical Wing Sections III, Springer-Verlag, Berlin, Heidelberg, New York, 1977.

[16] E. Stanewsky, W. Puffert-Meißner, R. Müller, H. Hoheisel, Der Transsonische Windkanal der DFVLR Braunschweig, DFVLR IB 129-82/4, 1982, to be published in ZfW.

[17] P.G. Wilby, Effect of Production Modifications to Rear of Westland Lynx Rotor Blade on Sectional Aerodynamic Characteristics, ARC-CP No. 1362, 1977.

[18] L. Dadone, US Army Helicopter Design DATCOM, Volume I - Airfoils, USAAMRDL CR 76-2, 1976.